NANO LETTERS

Letter

pubs.acs.org/NanoLett

Selecting for Function: Solution Synthesis of Magnetic Nanopropellers

Peter J. Vach,[†] Nicolas Brun,[‡] Mathieu Bennet,[†] Luca Bertinetti,[†] Marc Widdrat,[†] Jens Baumgartner,[†] Stefan Klumpp,[§] Peter Fratzl,[†] and Damien Faivre*[,†]

[†]Department of Biomaterials, [‡]Department of Colloid Chemistry, and [§]Department of Theory and Bio-Systems, Max Planck Institute of Colloids and Interfaces, Science Park Golm, 14424 Potsdam, Germany

Supporting Information

ABSTRACT: We show that we can select magnetically steerable nanopropellers from a set of carbon coated aggregates of magnetic nanoparticles using weak homogeneous rotating magnetic fields. The carbon coating can be functionalized, enabling a wide range of applications. Despite their arbitrary shape, all nanostructures propel parallel to the vector of rotation of the magnetic field. We use a simple theoretical model to find experimental conditions to select nanopropellers which are predominantly smaller than previously published ones.

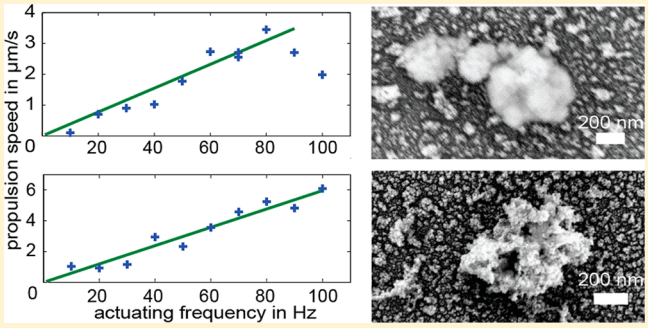

KEYWORDS: *Nanopropeller, self-assembly, magnetic nanoparticles, hydrodynamics, hydrothermal carbonization*

Micro- and nanostructures typically possess shape-dependent characteristics, like their optical,[1] catalytic,[2] or magnetic[3] properties. The typical approach to producing such structures in large quantities by solution synthesis is based on selection for shape. Reaction conditions and purification schemes are chosen to favor a specific shape.[4] A potentially more economical approach is to select instead for a specific function. This second option is particularly advantageous when the optimal shape is not known, or when a multitude of shapes can fulfill the desired function. Here we demonstrate this strategy by selecting magnetically steerable nanopropellers from a set of variedly shaped carbon coated aggregates of magnetic nanoparticles. Selecting for function can thus be a viable approach to producing functional nanoscopic devices in extremely large quantities.

Nanoscopic devices have the potential to manipulate biological and inanimate matter with unprecedented precision. Envisioned applications range from nanosurgery to the controlled assembly of microstructures.[5−7] Magnetic nanostructures are promising for such technologies, since they can be manipulated by external magnetic fields.[8−11] Unlike electric fields, magnetic fields are not screened by dissolved ions and can selectively exert large forces on magnetic materials. Gradient fields can in principle be used to directly actuate magnetic micro- and nanostructures,[12] but sufficiently strong gradient fields are difficult to produce. Coupling hydrodynamic forces with magnetic forces has allowed the creation of swimmers and propellers, which can be moved by weak homogeneous magnetic fields. Typical examples of swimmers are elastic structures driven by time-reversible magnetic fields,[13−16] whereas typical propellers are rigid structures actuated by nontime-reversible magnetic fields.[17,18] In fact, as described by the scallop theorem,[19] translatory movement would be impossible if both the actuating magnetic field was time-reversible and the structure rigid.

Previous micro- and nanopropellers were created using sophisticated nanofabrication methods[17,18,20] which allowed precise control of the propeller nanostructure but required expensive clean room equipment. In addition, such devices had at least one dimension larger than 1 μm, which might be too large for some of the envisioned applications.

Here we report the surprising finding that magnetically controllable nanopropellers with large dimensionless speeds can be selected from a diverse set of randomly shaped carbon-coated magnetic nanoparticle aggregates synthesized by a simple route. With specific experimental conditions we can predominantly select structures that are smaller than 1 μm in all dimensions. The nanopropellers are actuated, selected, and imaged in a custom-built open-frame microscope. Further characterization is performed by electron microscopy.

The synthesis method is based on hydrothermal carbonization (HTC), which has been used previously to coat iron oxide nanostructures.[21,22] In summary, we suspend iron oxide nanoparticles in glucose solution and heat it to 180 °C for 24 h. The HTC reaction leads to an efficient carbon coating of the iron oxide, effectively fixing the iron oxide nanoparticles in aggregates of varied shapes (Figures 4B and S5). A weak homogeneous rotating magnetic field is then used to select

Received: August 2, 2013
Revised: September 12, 2013
Published: October 15, 2013

   dx.doi.org/10.1021/nl402897x | *Nano Lett.* 2013, 13, 5373−5378

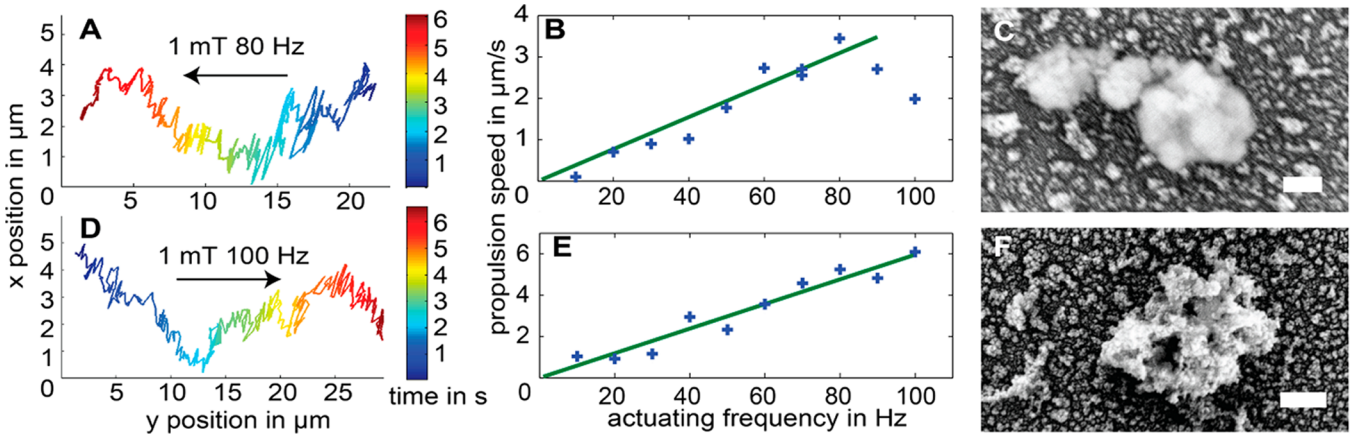

Figure 1. Two exemplary nanopropellers were first studied in the optical microscope. Two example traces of these measurements are displayed (A, D). The black arrows indicate the direction of the vector of rotation of the actuating magnetic field. Diffusive and translatory movements are superimposed. Speed versus frequency measurements show that the propulsion speed varies linearly with the frequency of the actuating magnetic field up to a critical frequency (around 80 Hz in B and above 100 Hz in E). Backscattered electron images of the two nanopropellers are displayed in panels C and F. Scale bars are 200 nm. The dimensionless speeds are estimated from these measurements as $U = 32$ ($v = 2.7$ µm s^{-1}, $L = 1.22$ µm, $f = 70$ Hz) for the upper nanopropeller (C) and $U = 69$ ($v = 6.1$ µm s^{-1}, $L = 0.88$ µm, $f = 100$ Hz) for the lower nanopropeller (F).

nanopropellers from the reaction product by letting them propel to the top of a glass vial (see Figure S1 for a schematic).

The direction of motion of the nanopropellers can be controlled, since they always move parallel to the vector of rotation of the magnetic field. The speed of the nanopropeller can also be controlled, by varying the frequency of the actuating field. We investigated the nanostructure of four typical nanopropellers with scanning electron microscopy (Figures 1 and S4). To this end we first measured the propulsion speed of a nanopropeller in a droplet on a marked coverslip and monitored the position of the nanopropeller during the drying process. The very same propeller was subsequently imaged with electron microscopy (Figure 1).

It is apparent that the nanopropellers are rather arbitrarily shaped and do not resemble the helical propellers published previously.[17,18] A helix with many turns might not be the optimal shape for a nanopropeller. This has recently been suggested by hydrodynamic simulations, which found a slender shape with about one helical turn to be optimal under certain assumptions.[23]

Different propellers can be compared using a dimensionless speed, defined as $U = v/(Lf) \times 10^3$, where v is the dimensional speed, L the largest dimension of the propeller, and f the frequency of the actuating magnetic field.[15] A propeller with particularly high dimensionless speed was created by glancing angle deposition,[18] with U up to 133 ($v = 40$ µm/s, $L = 2$ µm, $f = 150$ Hz). Self-scrolling thin films yielded a propeller[24] with U up to 21 ($v = 8$ µm/s, $L = 38$ µm, $f = 10$ Hz). A more recent propeller created by two-photon-lithography[25] achieved U up to 116 ($v = 93$ µm/s, $L = 35$ µm, $f = 23$ Hz). The exemplary propellers from our synthesis presented in Figure 1 have U values of 69 and 32, respectively.

In the following, we present a simple model we developed to describe the movement of our nanopropellers (Figure 2). We assume that the nanopropeller rotates around a given axis, independently of the actuating frequency. This could be due to a large magnetization of the nanopropeller, forced to rotate in the same plane as the magnetic field, or to the rotational friction coefficient being particularly low for a specific axis of rotation. With this assumption, we can describe the orientation of the nanostructure by a single angle φ and formulate the equations of motion. As we assume that the nanostructure always rotates around the same axis, the coupling between rotation and translation is constant. Thus:

$$v = c_v\dot{\varphi}$$

where v is the propulsion speed and c_v the coupling coefficient, which can be thought of as an effective screw pitch. Two torques act on the nanostructure, fluid friction τ_F and magnetic torque τ_M:

$$\tau_F = c_F\dot{\varphi}$$

$$\tau_M = BM\,\sin(\omega t - \varphi)$$

where c_F is the friction constant and M the magnetization of the nanopropeller. B and ω are the amplitude and frequency of the rotating magnetic field, respectively. In the strongly overdamped case of low Reynolds numbers, these torques must be equal at all times, and we get:

$$\dot{\varphi} = \frac{BM}{c_F}\sin(\omega t - \varphi)$$

An equivalent differential equation was recently derived and solved by Schamel and co-workers.[26] The full solution is complicated, but we obtain a rather simple expression for the dependence of the propulsion speed on the frequency of the actuating field

$$v(\omega) = \begin{cases} c_v\omega & \text{for } \omega < \omega_c \\ c_v\left(\omega - \sqrt{\omega^2 - \omega_c^2}\right) & \text{for } \omega > \omega_c \end{cases}$$

where we call $\omega_c = BM/c_F$ the critical frequency (see SI, part 2). Figure 2 B shows that this prediction is in good agreement with experimental observation.

Our hydrodynamic model of the nanopropeller motion treats water as a continuous viscous fluid and ignores the effect of thermal noise. However, the nanopropellers presented here are small enough for significant Brownian motion to occur (Figure 1A and D and Figure 3 A). We did not include thermal noise in our model, since we assume that Brownian motion is simply superimposed on the nanopropeller propulsion and cancels out

dx.doi.org/10.1021/nl402897x | Nano Lett. 2013, 13, 5373−5378

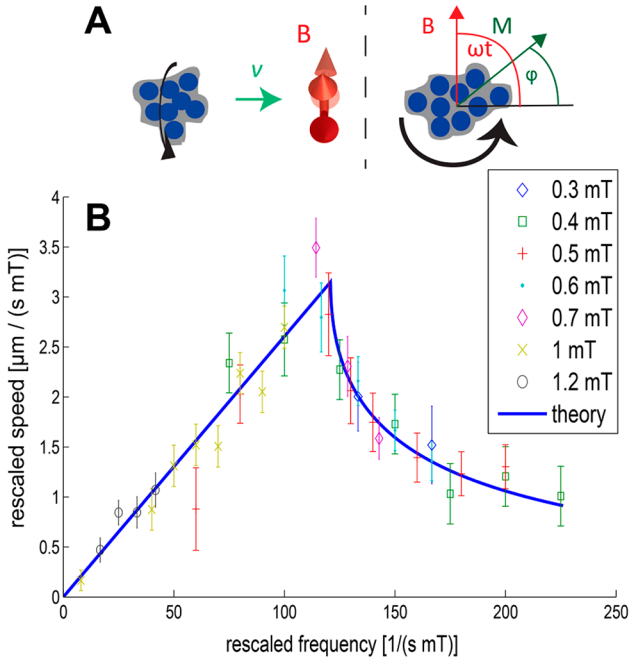

Figure 2. (A) Scheme illustrating our theoretical model and the variables used. On the left the propulsion speed v is drawn parallel to the vector of rotation of the turning magnetic fields. The red arrows indicate a time series of magnetic field vectors. Turning this schematic out of the plane, we arrive at the scheme on the right. The magnetic field B and the magnetic moment M are indicated as well as the angle φ that is used to describe the orientation of the nanopropeller, relative to the magnetic field vector which is rotating at the frequency ω. (B) For one individual nanopropeller (imaged in Figure S5 I), the propulsion speed was measured at various magnetic field strengths and frequencies. The speed divided by the magnetic field strength is plotted against the frequency divided by the magnetic field strength. Error bars are based on the expected standard deviation of the end position measurement due to diffusion. The diffusion constant was measured to be 0.9 $\mu m^2\ s^{-1}$ (see SI, part 4). The theoretically expected curve is plotted in blue. Two parameters were determined by nonlinear regression: c_v = 26.1 nm and B/ω_c = 8.27 mT ms. This measurement is more precise than the one shown in Figure 1, as speed measurements could here be performed in bulk water, far away from a potentially disturbing surface.

on average. To show the validity of this assumption, we split nanopropeller trajectories into a propulsion and a noise component by linear fits of the x and y data (Figure 3A). This was done for trajectories with different nanopropeller speeds, respectively above and below the critical frequency of the nanopropeller. The noise components obtained in this way were used to calculate diffusion constants (Figure 3B), which were similar to that obtained from a high speed video of the nanopropeller diffusing with the magnetic field switched off (Figure S3). Another characteristic property of Brownian motion is that the absolute value of its Fourier transform decreases as $|\mathcal{F}(y_B)| \propto f^{-1}$, where $\mathcal{F}(y_B)$ denotes the Fourier transform of a time series of y positions and f is the frequency. We fitted functions of the form af^b (a and b constants) to the noise components of different trajectories and always obtained b values close to one (Figure 3C). At high frequencies we observed slightly higher noise than expected from Brownian motion, which is probably due to additional noise produced by the limited precision of the tracking algorithm. We therefore conclude that we can indeed describe nanopropeller motion as

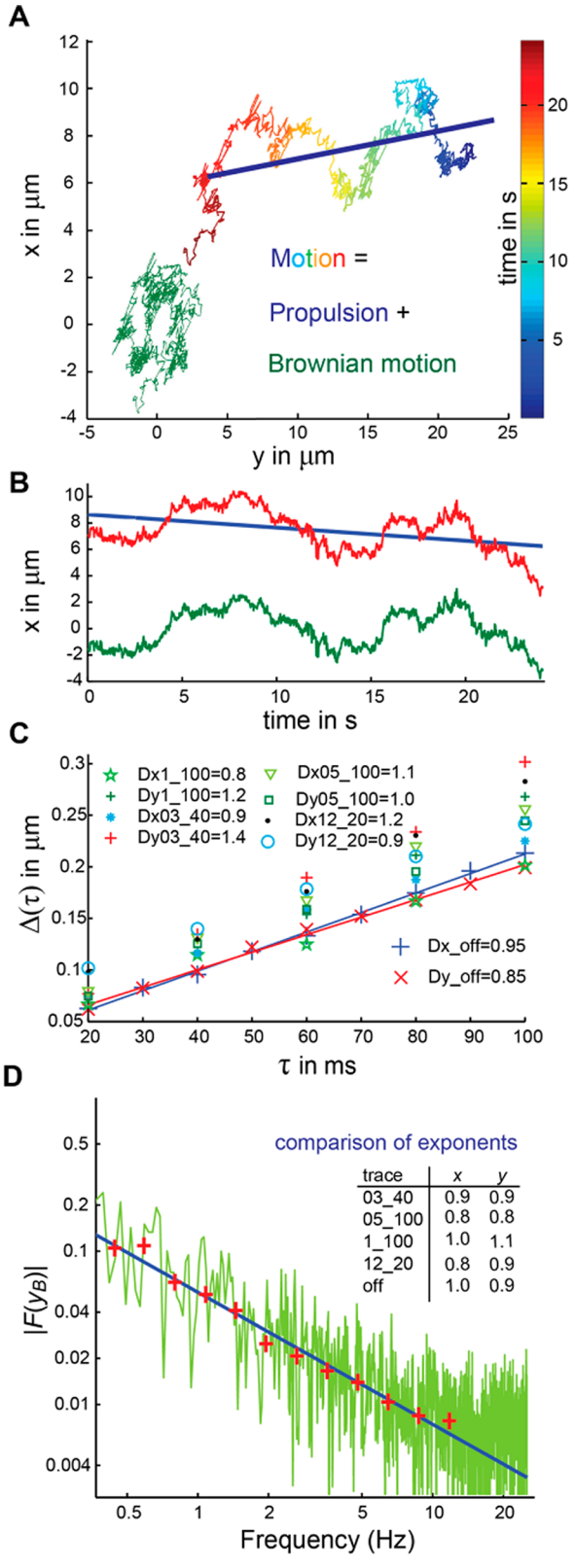

Figure 3. Decomposition of the motion of the nanopropeller into a propulsion component described by our theoretical model and a noise component that can be described as Brownian motion. All data stem from measurements of the nanopropeller displayed in Figure S5 I. (A) Trace of the nanopropeller moving in a 0.3 mT field rotating at 40 Hz (see Supplementary Movie 4). The propulsion is slow as the propeller is actuated above its critical frequency. By fitting linear functions to the x and y components of the trajectory, the trace can be split into a

dx.doi.org/10.1021/nl402897x | Nano Lett. 2013, 13, 5373−5378

Figure 3. continued

propulsion component (in blue) and a noise component (in green). Adding these components reproduces the original trace. (B) The splitting procedure is exemplified for the x coordinate of the same trace (in red). The propulsion component is a linear fit (in blue). The difference between the two is the noise component (in green). Splitting of the y coordinate is done equivalently. (C) Determination of the diffusion coefficient based on the noise components of various traces. $\Delta(\tau)$ is the width of a Gaussian fit to the distribution of distances, traversed during a time τ (see Figure S3). A linear fit yields an estimate for the diffusion coefficient.[27] The obtained diffusion coefficients are displayed with the data labels, whereby the first number denotes the field strength and the second number the frequency. The Supplementary Videos, in which these traces can be observed, are labeled in the same way. The fact that the noise component data allow this analysis is a strong indication that the origin of the noise component is Brownian motion. The diffusion coefficients are very similar to the values obtained from a high speed measurement with the magnetic field turned off. The biggest discrepancy is observed in trace03_40, which is the reason we display it in this figure. (D) The absolute value of the Fourier transform of the y noise component of trace03_40 is plotted against the frequency in a log–log plot. After binning the data (red crosses) we can fit a straight line (in blue). The negative of the slope of this line is an exponent, which is expected to be 1 for Brownian motion. The inset shows that the fitted exponents for the noise components of all traces are close to 1.

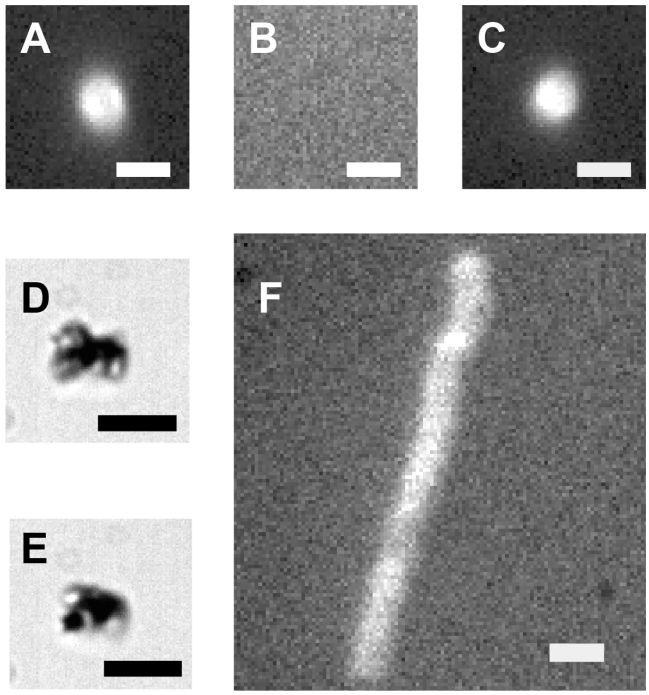

Figure 5. (A) Fluorescence image of a labeled propeller moving toward the upper inner surface of a glass capillary, actuated by a magnetic field of 1 mT rotating at 50 Hz. (B) When the magnetic field is switched off, the same nanopropeller falls out of focus, and the fluorescence disappears. (C) When the field is switched back on, this nanopropeller returns to the upper inner surface of the capillary and is visible again. Panels D and E show brightfield images of this propeller in different orientations. Panel F shows the movement of this propeller along the lower surface of the capillary during 7 s exposure time. Scale bars are 4 μm.

a superposition of our hydrodynamic model and Brownian motion.

Based on our theoretical work, we expect smaller nanopropellers to have a higher critical frequency (see SI, part 6c). This expectation was confirmed by optical size estimates of propellers that could propel to the upper inner surface of a capillary in rotating magnetic fields of different field strengths (Figure 4A). Indeed, fewer larger structures can propel upward, against gravity, in a weaker magnetic field. To study the smallest propellers, we acquired backscattered electron micrographs to image structures selected with a reduced magnetic field of 0.5 mT rotating at 100 Hz. We found structures smaller than 1 μm (Figure 4B), showing that nanopropellers can be selected from our synthesis products. The smallest propellers we observed were around 300 nm in size. For comparison, the smallest propellers previously reported measured about 1.5 μm along their longest dimension.[18]

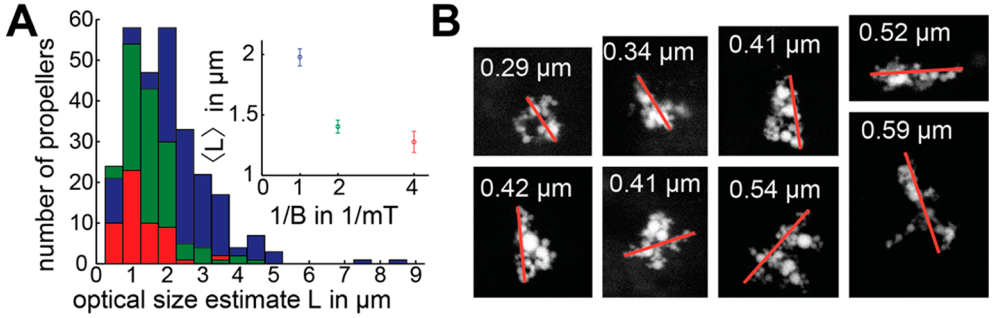

Figure 4. (A) Size distribution of propellers selected in different rotating magnetic fields (red 0.25 mT, green 0.5 mT, blue 1 mT, frequency always 100 Hz). Synthesized nanostructures of a fixed concentration were injected (without prior selection) into a glass capillary and subjected to a rotating magnetic field. A fixed area of the upper, inner surface of the capillary was imaged, while the rotating magnetic field was continuously applied. The histograms display the total number of structures of a particular size that were found to propel against gravity in the applied rotating magnetic field. As expected from our theory, fewer larger structures can propel upward in a weaker magnetic field. This is also apparent in the inset, where the mean size is plotted against the inverse magnetic field strength (error bars are standard error). Our size estimation is based on optical images; therefore its accuracy is limited by diffraction, which is particularly apparent for nanopropellers smaller than 1 μm. (B) To study the smallest propellers, we acquired backscattered electron images of structures that were selected in a 0.5 mT, 100 Hz magnetic field. Based on the distance traveled and the duration of our selection experiment, we can estimate the dimensionless speed value of a nanopropeller of 1 μm size to be above 10, for propulsion against gravity. This minimal dimensionless speed is proportionally larger for smaller nanopropellers. Here we report the eight smallest structures we observed. More images of nanopropellers are presented in Figure S5.

dx.doi.org/10.1021/nl402897x | *Nano Lett.* 2013, 13, 5373–5378

Many potential applications rely on functionalizing the propeller's surface. The carboxylic groups present on HTC carbon[28] allow such surface modification. We demonstrate this ability by fluorescently labeling our nanostructures (Figure 5).

Our functionalization technique is versatile and can enable a wide range of applications such as controlled assembly in solution[7] or triggered release.[29] Other potential applications include fluid mixing at low Reynolds numbers and local rheological probes.[10] Production of our nanopropellers is simple, cheap, and scalable and thus of particular interest to large-scale applications, such as micropatterning of large surfaces[30] and environmental remediation.[31]

The general idea of selecting from randomness has been previously demonstrated for libraries of chemical compounds (combinatorial chemistry) or viral proteins (phage display), thereby showing great potential. We demonstrated here that this principle can also be used for the selection of nanopropellers with specific properties. Such an approach might also be successfully applied to other combinations of external stimuli and random features.

■ ASSOCIATED CONTENT

Ⓢ Supporting Information

Detailed experimental methods, additional theoretical considerations, author contributions, supplementary figures, and supplementary videos. This material is available free of charge via the Internet at http://pubs.acs.org.

■ AUTHOR INFORMATION

Corresponding Author

*E-mail: damien.faivre@mpikg.mpg.de.

Notes

The authors declare no competing financial interest.

■ ACKNOWLEDGMENTS

Magdalena Titirici is acknowledged for discussions. The research was supported by the Max Planck Society and the ERC through a starting grant to D.F. (256915-MB2).

■ REFERENCES

(1) Kelly, K. L.; Coronado, E.; Zhao, L. L.; Schatz, G. C. The optical properties of metal nanoparticles: the influence of size, shape, and dielectric environment. *J. Phys. Chem. B* **2003**, *107*, 668−677.

(2) Narayanan, R.; El-Sayed, M. A. Shape-dependent catalytic activity of platinum nanoparticles in colloidal solution. *Nano Lett.* **2004**, *4*, 1343−1348.

(3) Muxworthy, A. R.; Williams, W. Critical single-domain/multidomain grain sizes in noninteracting and interacting elongated magnetite particles: Implications for magnetosomes. *J. Geophys. Res.* **2006**, *111*, B12S12.

(4) Sau, T. K.; Rogach, A. L. Nonspherical Noble Metal Nanoparticles: Colloid-Chemical Synthesis and Morphology Control. *Adv. Mater.* **2010**, *22*, 1781−1804.

(5) Mavroidis, C.; Ferreira, A. Special Issue on Current State of the Art and Future Challenges in Nanorobotics. *Int. J. Robot. Res.* **2009**, *28*, 419−420.

(6) Sitti, M. Miniature devices: Voyage of the microrobots. *Nature* **2009**, *458*, 1121−1122.

(7) Martel, S.; Mohammadi, M. Using a swarm of self-propelled natural microrobots in the form of flagellated bacteria to perform complex micro-assembly tasks. *Robotics and Automation (ICRA), 2010 IEEE International Conference*, Anchorage, Alaska, May 3−8, 2010; pp 500−505.

(8) Erb, R. M.; Son, H. S.; Samanta, B.; Rotello, V. M.; Yellen, B. B. Magnetic assembly of colloidal superstructures with multipole symmetry. *Nature* **2009**, *457*, 999−1002.

(9) Khalil, K. S.; Sagastegui, A.; Li, Y.; Tahir, M. A.; Socolar, J. E. S.; Wiley, B. J.; Yellen, B. B. Binary colloidal structures assembled through Ising interactions. *Nat. Commun.* **2012**, *3*, 794.

(10) Fischer, P.; Ghosh, A. Magnetically actuated propulsion at low Reynolds numbers: towards nanoscale control. *Nanoscale* **2011**, *3*, 557−563.

(11) Zhang, L.; Peyer, K. E.; Nelson, B. J. Artificial bacterial flagella for micromanipulation. *Lab Chip* **2010**, *10*, 2203−2215.

(12) Zeeshan, M. A.; Pané, S.; Youn, S. K.; Pellicer, E.; Schuerle, S.; Sort, J.; Fusco, S.; Lindo, A. M.; Park, H. G.; Nelson, B. J. Graphite Coating of Iron Nanowires for Nanorobotic Applications: Synthesis, Characterization and Magnetic Wireless Manipulation. *Adv. Funct. Mater.* **2013**, *23*, 823−831.

(13) Dreyfus, R.; Baudry, J.; Roper, M. L.; Fermigier, M.; Stone, H. A.; Bibette, J. Microscopic artificial swimmers. *Nature* **2005**, *437*, 862−865.

(14) Gao, W.; Sattayasamitsathit, S.; Manesh, K. M.; Weihs, D.; Wang, J. Magnetically Powered Flexible Metal Nanowire Motors. *J. Am. Chem. Soc.* **2010**, *132*, 14403−14405.

(15) Pak, O. S.; Gao, W.; Wang, J.; Lauga, E. High-speed propulsion of flexible nanowire motors: Theory and experiments. *Soft Matter* **2011**, *7*, 8169−8181.

(16) Benkoski, J. J.; Breidenich, J. L.; Uy, O. M.; Hayes, A. T.; Deacon, R. M.; Land, H. B.; Spicer, J. M.; Keng, P. Y.; Pyun, J. Dipolar organization and magnetic actuation of flagella-like nanoparticle assemblies. *J. Mater. Chem.* **2011**, *21*, 7314−7325.

(17) Zhang, L.; Abbott, J. J.; Dong, L.; Peyer, K. E.; Kratochvil, B. E.; Zhang, H.; Bergeles, C.; Nelson, B. J. Characterizing the Swimming Properties of Artificial Bacterial Flagella. *Nano Lett.* **2009**, *9*, 3663−3667.

(18) Ghosh, A.; Fischer, P. Controlled Propulsion of Artificial Magnetic Nanostructured Propellers. *Nano Lett.* **2009**, *9*, 2243−2245.

(19) Purcell, E. M. Life at low Reynolds number. *Am. J. Phys.* **1977**, *45*, 3−11.

(20) Ghosh, A.; Paria, D.; Singh, H. J.; Venugopalan, P. L.; Ghosh, A. Dynamical configurations and bistability of helical nanostructures under external torque. *Phys. Rev. E* **2012**, *86*, 031401.

(21) Zhang, Z.; Duan, H.; Li, S.; Lin, Y. Assembly of Magnetic Nanospheres into One-Dimensional Nanostructured Carbon Hybrid Materials. *Langmuir* **2010**, *26*, 6676−6680.

(22) Zhang, W.-M.; Wu, X.-L.; Hu, J.-S.; Guo, Y.-G.; Wan, L.-J. Carbon Coated Fe_3O_4 Nanospindles as a Superior Anode Material for Lithium-Ion Batteries. *Adv. Funct. Mater.* **2008**, *18*, 3941−3946.

(23) Keaveny, E. E.; Walker, S. W.; Shelley, M. J. Optimization of Chiral Structures for Microscale Propulsion. *Nano Lett.* **2013**, *13*, 531−537.

(24) Zhang, L.; Abbott, J. J.; Dong, L.; Kratochvil, B. E.; Bell, D.; Nelson, B. J. Artificial bacterial flagella: Fabrication and magnetic control. *Appl. Phys. Lett.* **2009**, *94*, 064107−064103.

(25) Tottori, S.; Zhang, L.; Qiu, F.; Krawczyk, K. K.; Franco-Obregón, A.; Nelson, B. J. Magnetic Helical Micromachines: Fabrication, Controlled Swimming, and Cargo Transport. *Adv. Mater.* **2012**, *24*, 811−816.

(26) Schamel, D.; Pfeifer, M.; Gibbs, J. G.; Miksch, B.; Mark, A. G.; Fischer, P. Chiral Colloidal Molecules and Observation of the Propeller Effect. *J. Am. Chem. Soc.* **2013**, *135*, 12353−12359.

(27) Crocker, J. C.; Grier, D. G. Methods of digital video microscopy for colloidal studies. *J. Colloid Interface Sci.* **1996**, *179*, 298−310.

(28) Titirici, M.-M.; White, R. J.; Falco, C.; Sevilla, M. Black perspectives for a green future: hydrothermal carbons for environment protection and energy storage. *Energy Environ. Sci.* **2012**, *5*, 6796−6822.

(29) Giri, S.; Trewyn, B. G.; Stellmaker, M. P.; Lin, V. S. Y. Stimuli-Responsive Controlled-Release Delivery System Based on Mesoporous Silica Nanorods Capped with Magnetic Nanoparticles. *Angew. Chem., Int. Ed.* **2005**, *44*, 5038−5044.

(30) Manesh, K. M.; Campuzano, S.; Gao, W.; Lobo-Castañón, M. J.; Shitanda, I.; Kiantaj, K.; Wang, J. Nanomotor-based biocatalytic patterning of helical metal microstructures. *Nanoscale* **2013**, *5*, 1310−1314.
(31) Zhu, J.; Wei, S.; Chen, M.; Gu, H.; Rapole, S. B.; Pallavkar, S.; Ho, T. C.; Hopper, J.; Guo, Z. Magnetic nanocomposites for environmental remediation. *Adv. Powder Technol.* **2013**, *24*, 459−467.

dx.doi.org/10.1021/nl402897x | *Nano Lett.* 2013, 13, 5373−5378